

Dipole phase and photoelectron group delay in inner shell photoionization

A. S. Kheifets*

Research School of Physics and Engineering, The Australian National University, Canberra ACT 0200, Australia

V. K. Dolmatov

Department of Physics and Earth Science, University of North Alabama, Florence, AL 35632, USA

S. Saha, P. C. Deshmukh

Department of Physics, Indian Institute of Technology Madras, Chennai-600036, India

D. A. Keating, S. T. Manson

Department of Physics and Astronomy, Georgia State University, Atlanta, 30303, U.S.A.

(Dated: September 22, 2015)

We conduct a systematic study of the dipole phase and the photoelectron group delay (Wigner time delay) in inner shell photoionization of noble gas atoms from Ne to Xe. Our study encompasses the tender X-ray spectral range and extends to 1 keV photoelectron energy. We employ both the relativistic and non-relativistic versions of the random phase approximation with exchange. We identify the long range Coulomb and short range Hartree-Fock contributions to the dipole phase which governs the Wigner time delay variation from the threshold to the whole range of photoelectron energies.

PACS numbers: 32.80.Aa 32.80.Fb 32.80.RM 32.80.Zb 42.50.Hz

I. INTRODUCTION

The availability of time synchronized XUV pump and IR probe laser pulses has allowed for the accurate determination of the phase of the dipole photoionization amplitude (matrix element). In the attosecond streaking technique, an isolated XUV pump pulse is superimposed with a phase-locked IR probe to convert the relative XUV/IR phase into the kinetic energy of the photoelectron [1]. This conversion is used to obtain the timing of the photoelectron wave packet release [2]. The latter can be interpreted in terms of the photoelectron group delay (also known as the Wigner time delay or the Wigner-Eisenbud-Smith time delay [3–5]). The alternative RABBITT technique employs an attosecond pulse train as a pump superimposed with a spectrally narrow IR probe to Reconstruct the Attosecond Beatings caused By Interference of Two-photon Transitions [6]. The phase of these beatings encodes the dipole photoionization amplitude phase which again can be converted to the Wigner time delay [7, 8]. Yet another alternative method to reconstruct the photoionization phase is the high-harmonic generation (HHG) technique. Because photorecombination is the inverse process to photoionization, their phases are identical. The photorecombination phase is encoded in the spectral phase of the harmonic comb and can be retrieved using the RABBITT technique [9] or harmonic spectroscopy based on two-color driving pulses [10].

So far, these phase retrieval techniques have been exploited in the XUV spectral range not significantly ex-

ceeding the photon energy of 100 eV. Recent experiments with mid-IR driving pulses allowed the extension of the harmonic emission to much higher photon energies [11, 12]. This extension allows the study of photoemission processes in inner atomic shells and the retrieval of the phase and timing information. At the same time, accurate modeling of the HHG process in this spectral range requires knowledge of the photo-recombination amplitude phase which has been unavailable in the literature so far [13].

A parallel development, which allows potentially the study of photoionization phase over an extended spectral range, is the streaking of a free-electron laser (FEL) radiation with a THz probe [14, 15]. The same idea of the THz streak camera allows for a high-precision measurement of the arrival time of an FEL pulse [16–18]. The photoionization time delay is also needed for understanding the energy spectra of the photoelectrons created by the FEL pulses [19]. These spectra do not exactly mimic the spectrum of the photon pulse, rather their spectrum is a convolution of the photon pulse spectrum and the emission spectrum corresponding to the ionization time. Depending on the ionization time and the temporal structure of the FEL pulse, the spectrum of the electrons can be dominated by one of these components.

To address these needs, we conduct a systematic study of the dipole photoionization phase and the Wigner time delay in inner shells of the noble gas atoms from Ne to Xe. This study encompasses the tender x-ray spectral range and extends to 1 keV photoelectron energy. This includes K, L shells of Ne, K, L, M shells of Ar and L, M shells of Kr and Xe (see Table I for respective binding energies). The present study partially overlaps with, and is complementary to, our previous work [20] where time

*Electronic address: A.Kheifets@anu.edu.au

delay in valence shell photoionization of noble gases was investigated.

TABLE I: Electron binding energies, in electron volts, as collated in the X-ray data booklet [21]

	K	LI	LII	LIII	MI	MII	MIII	MIV	MV
	1s	2s	2p _{1/2}	2p _{3/2}	3s	3p _{1/2}	3p _{3/2}	3d _{3/2}	3d _{5/2}
Ne	870.2	48.5	21.7	21.6					
Ar	3,206	326.3	250.6	248.4	29.3	15.9	15.7		
Kr	14,326	1,921	1,731	1,678	292.8	222.2	214.4	95.0	93.8
Xe	34,561	5,453	5,107	4,786	1,149	1,002	940.6	689.0	676.4

Our methodology (Sec. II) is similar to the previous works [20, 22] and employs both non-relativistic and relativistic versions of the random phase approximation with exchange (RPAE and RRPA, respectively). As test of accuracy, we compare our calculated subshell photoionization cross-sections with the literature values collated by Berkowitz [23] for Ne, Ar and Kr and calculated by Band et al. [24] for Xe (Sec. III A). Satisfied with these tests, we proceed with the photoionization amplitude phase calculation (Sec. III B). We compare the phase results from correlated RPAE calculations with those from the single-electron Hartree-Fock (HF) approximation. Thus we can identify clearly the effect of many-electron correlation. Then we convert the phase into the Wigner time delay calculated in the direction of the polarization of the XUV radiation (Sec. III C). We do not evaluate the corrections induced by the coupling of the long-range Coulomb ionic potential and the streaking field (CLC corrections). These corrections are of universal nature and can be found in the literature [25, 26]. Finally, we elucidate the role of relativistic effects by making comparison of the time delay results from the RPAE and RRPA calculations (Sec. III D)

II. THEORETICAL METHOD AND COMPUTATION DETAILS

For the non-relativistic RPAE, we follow closely the photoionization formalism as outlined in our previous work [20]; the relativistic RRPA development is essentially the same, but based on the Dirac equation rather than the Schrödinger equation. Here we reproduce only few essential details to benefit the reader. We evaluate the one-photon dipole matrix element $\langle \psi_k^{(-)} | \hat{z} | \phi_i \rangle$ from a bound state $\phi_i(r) = Y_{l_i m_i}(\hat{r}) R_{n_i l_i}(r)$ to an incoming scattering state with the given photoelectron momentum k :

$$\psi_k^{(-)}(r) = \frac{(2\pi)^{3/2}}{k^{1/2}} \sum_{lm} i^l e^{-i\delta_l(E)} Y_{lm}^*(\hat{k}) Y_{lm}(\hat{r}) R_{kl}(r). \quad (1)$$

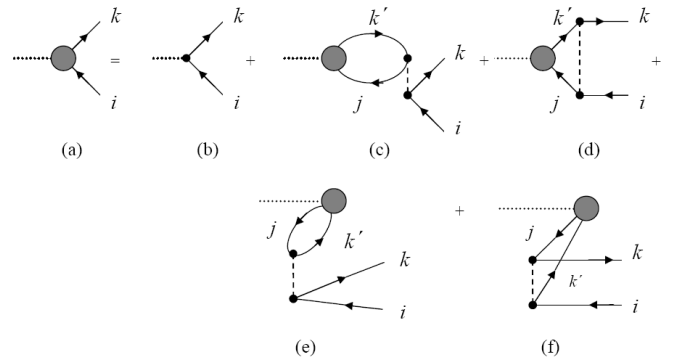


FIG. 1: Diagrammatic representation of the photoionization amplitude $\langle kl | \hat{D} | n_i l_i \rangle$ in the RPAE. Here, the time axis is directed from the left to right, the lines with arrows to the left (right) correspond to holes (electrons) in a filled atomic shell, a dotted line represents an incoming photon, a dashed line represents the Coulomb interaction between charged particles, and a shaded circle marks the effective operator \hat{D} for the photon-atom interaction which accounts for electron correlation in the atom.

We conduct the spherical integration to arrive to the following expression:

$$\langle \psi_k^{(-)} | \hat{z} | \phi_i \rangle = \frac{(2\pi)^{3/2}}{k^{1/2}} \sum_{\substack{l=l_i \pm 1 \\ m=m_i}} e^{i\delta_l(E)} i^{-l} Y_{lm}(\hat{k}) \quad (2) \\ \times \begin{pmatrix} l & 1 & l_i \\ m & 0 & m_i \end{pmatrix} \langle kl | \hat{D} | n_i l_i \rangle$$

Here $\langle kl | \hat{D} | n_i l_i \rangle$ is the reduced dipole matrix element, stripped of all the angular momentum projections. The partial photoionization cross section for the transition from an occupied state $n_i l_i$ to the photoelectron continuum state kl is calculated as

$$\sigma_{n_i l_i \rightarrow kl}(\omega) = \frac{4}{3} \pi^2 \alpha a_0^2 \omega \left| \langle kl | \hat{D} | n_i l_i \rangle \right|^2, \quad (3)$$

α being the fine structure constant and a_0 the Bohr radius Atomic units $e = m = \hbar = 1$ are used in this expression and throughout the paper.

In the independent electron Hartree-Fock (HF) approximation, the reduced dipole matrix element is evaluated as a radial integral,

$$\langle kl | \hat{D} | n_i l_i \rangle = \hat{u}_i \begin{pmatrix} l & 1 & l_i \\ 0 & 0 & 0 \end{pmatrix} \int r^2 dr R_{kl}(r) r R_{n_i l_i}(r), \quad (4)$$

where the hat symbol $\hat{l} = \sqrt{2l+1}$ is used. The basis of occupied atomic states $|n_i l_i\rangle$ is defined by the self-consistent HF method and calculated using the computer code [27]. The continuum electron orbitals $\langle kl |$ are defined within the frozen-core HF approximation and evaluated using the computer code [28].

In the random phase approximation with exchange (RPAE), the reduced dipole matrix element is found by

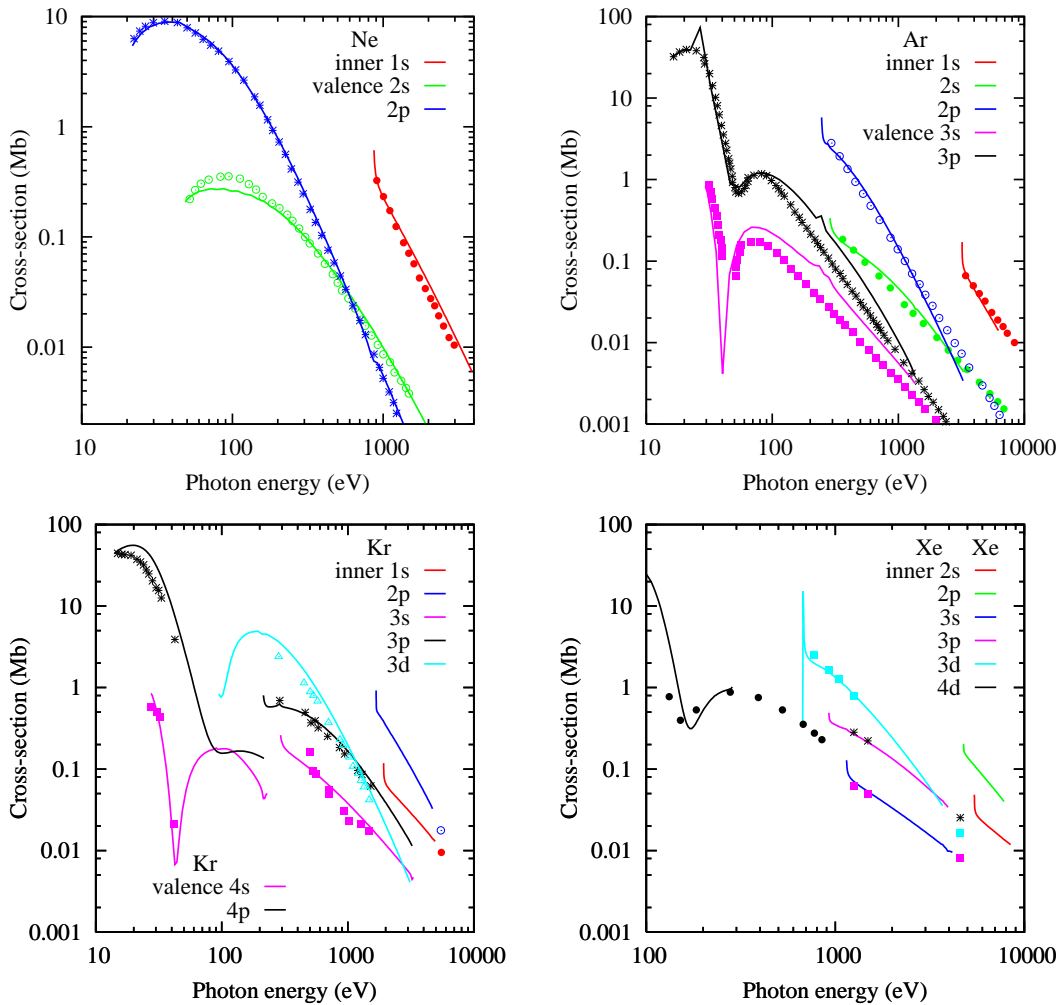


FIG. 2: (Color online) Shell photoionization cross-sections of Ne, Ar, Kr and Xe from non-relativistic RPAE calculations are shown with lines. Similarly colored dots represent the literature values collated by Berkowitz [23] for Ne, Ar and Kr and calculated by Band et al. [24] for Xe

summing an infinite sequence of Coulomb interactions between the photoelectron and the hole in the ionized shell. This leads to a system of integral equations which can be represented graphically by the diagrams of Fig. 1.

There, diagram (a) represents the sum of all Coulomb interactions, diagram (b) depicts the HF term given by Eq. (4) and diagrams (c)–(f) represent RPAE corrections. Diagrams (c) and (d) are known as time direct (forward) and (e) and (f) as time reverse (backward). Diagrams (d) and (f) account for the exchange interaction in the atom, thus being called the exchange diagrams. As is

seen from Fig. 1, a virtual excitation in the shell j to the ionized electron state k' may affect the final ionization channel from the shell i . This way RPAE accounts for the effect of inter-shell $i \leftrightarrow j$ correlation.

The photoelectron group delay, which is the energy derivative of the phase of the complex photoionization amplitude, is evaluated as

$$\tau = \frac{d}{dE} \arg f(E) \equiv \text{Im} \left[\frac{f'(E)}{f(E)} \right]. \quad (5)$$

Here $f(E)$ is given by Eq. (2) with $E = k^2/2$ and $\hat{k} \parallel z$.

III. RESULTS AND DISCUSSION

A. Shell photoionization cross-sections

The partial (shell) photoionization cross-sections from RPAE calculations are displayed in Fig. 2 for Ne and Ar

(top) and Kr and Xe (bottom). The present calculated results are compared with experimental values collated by Berkowitz [23] for Ne, Ar and Kr, and calculated by Band et al. [24] for Xe. Agreement with the literature data is good for inner shells but some deviation is visible for the valence shells. This deviation may be due to stronger inter-shell correlations than is accounted for by the RPAE. But, the inner shells are tightly bound by the nucleus and their electron states are well described by the independent electron HF approximation. Note further, that our RRPA results are essentially identical to the RPAE results on the scale shown in Fig. 2.

B. Phase analysis

The phases of the dipole photoionization amplitude $\arg f(E)$, as calculated in the RPAE, are displayed in Fig. 3 for Ne and Ar (top) and Kr and Xe (bottom). To demonstrate the effect of correlation, primarily in the form of interchannel coupling, the RPAE phases are compared with the HF results. Note that these are the total phases of the dipole amplitudes including the Coulomb phases. At the HF level, the reduced matrix element, Eq.(4) is real and thus the phase of the complex dipole matrix element, Eq. (2), is defined by the scattering phases $\delta_{l_i \pm 1}(E)$. According to the Fano's propensity rule [29], the dipole transition with the increased momentum $l = l_i + 1$ is usually dominant. In such a situation, $\arg f(E) \simeq \delta_{l_i+1}(E)$. It is this phase that is labeled as HF in the legend of Fig. 3.

The scattering potential acting upon the photoelectron is the sum of the Coulomb field of the nucleus and the HF potential of the frozen electron core of the residual ion. So the photoelectron scattering phase $\delta_l(E)$ contains both the long-range Coulomb and the short-range Hartree-Fock components. The Coulomb phase is given by the expression $\sigma_l(E) = \arg \Gamma(1 + l + i\eta)$ where the Sommerfeld parameter $\eta = -z/\sqrt{2E}$ is determined by the final state ionic charge; for photoionization of neutral atoms, $z \equiv 1$. The Coulomb phase at small photoelectron energy diverges [30]:

$$\sigma_l(E) \simeq \eta \left[\ln \sqrt{(l+1)^2 + \eta^2} - 1 \right] \rightarrow \eta \ln |\eta|. \quad (6)$$

The phase shift due to the short range potential, i.e. the

difference of the total phase and the Coulomb phase, is related to the asymptotic quantum defect μ according to the Levinson-Seaton theorem $\delta_L(E \rightarrow 0) - \sigma_L(E \rightarrow 0) = \mu_\infty \pi$ [31] where E is the photoelectron energy.

The asymptotic quantum defects μ_∞ are obtained for the various $\underline{n_i l_i n l}$ Rydberg series using

$$E_{\underline{n_i l_i n l}} = -\frac{Z_{\text{eff}}^2}{(n - \mu_\infty)^2}, \quad Z_{\text{eff}} = 1, \quad n \rightarrow \infty$$

where $E_{\underline{n_i l_i n l}}$ is the energy of the state $n_i l_i^{-1} n l$ (in Rydbergs) with respect to the $n_i l_i^{-1}$ threshold of the ion; the results are shown in Table II. When analyzing these results, one should bear in mind that for a neutral target, the scattering phase at zero energy is related to the number of the bound target states of angular momentum l , N_l , by Levinson's theorem, $\delta_l(k \rightarrow 0) = N_l \pi$. Looking at the table, we see indeed that for lighter atoms generally $\mu \sim N_l$. For instance, in the ionic core of Ne^+ , there is one occupied $2p$ orbital and no nd orbitals. Hence the short-range phase tends to one unit of π for $1s$ and $2s$ shell photoionization and to zero for $2p$ photoionization. As the number of occupied shells grows from Ne to Xe, same increase in the μ parameters can be seen in the table. In the meantime, in Kr and Xe the number of occupied d shells is mismatched by one unit from the quantum defect. This reinforces the idea that Levinson's theorem applies only very approximately to positive ions.

In the same Table II, we show the results of the logarithmic fit to the RPAE phase at large photoelectron energies

$$\arg f(E) \propto a - \frac{1}{c} \ln E(\text{eV}) \quad (7)$$

The a parameter in this fit corresponds to the phase at the photoelectron energy $E = 1$ eV and a/π may be compared with quantum defect parameter μ . This comparison made in Table II shows a close correspondence between the two parameters μ and a/π for the various np series, and some of the nd series; these are the channels where the short-range HF phase is monotone decreasing from threshold Kennedy and Manson [32]. In the other nd channels, along with the nf channel, there are significant shape resonances in the threshold region so the extrapolation fails.

Comparison of the RPAE and HF phases in Fig. 3 shows that for the inner shells, especially in heavier atoms, these two calculations produce very similar re-

sults. This means that the role of the correlation is limited for the inner shell photoionization processes. Indeed, the inner shell electrons are tightly bound by the

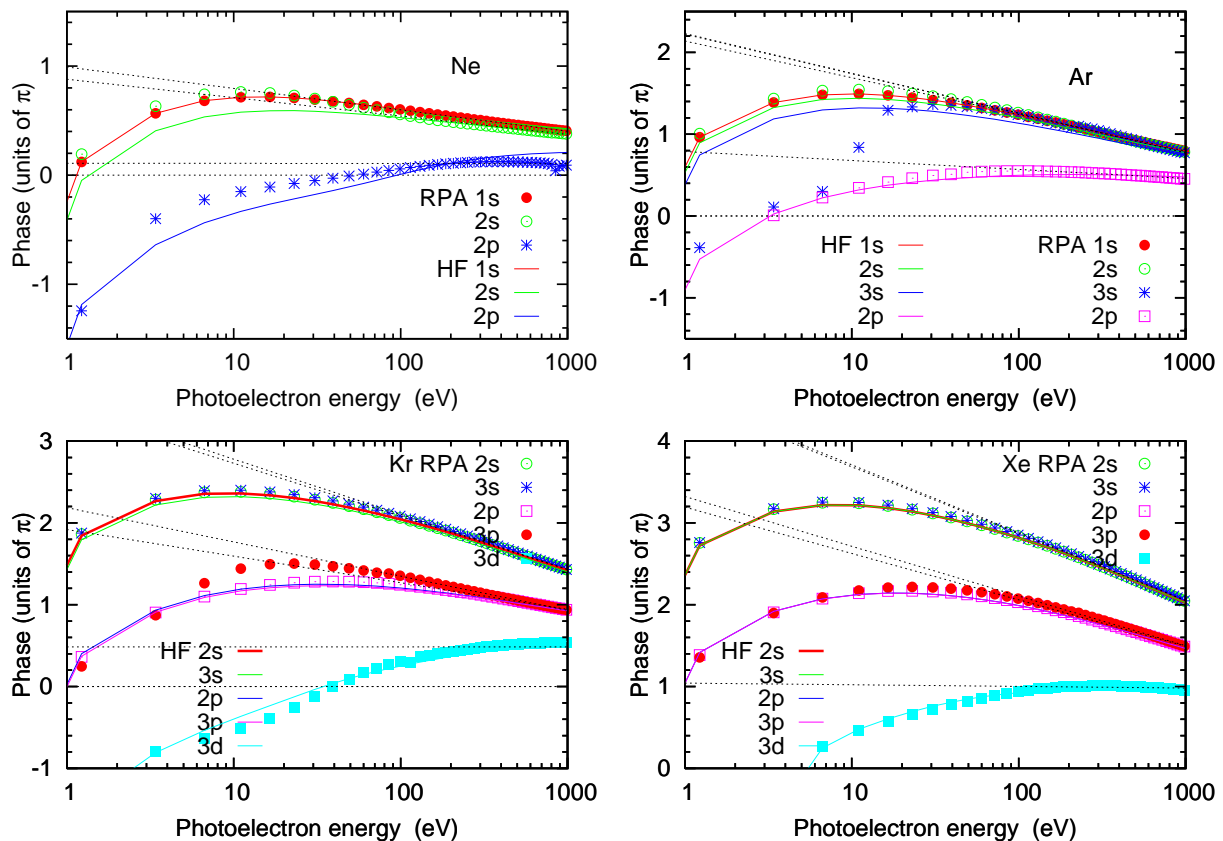


FIG. 3: (Color online) Phases of the photoionization amplitude in various shells of Ne, Ar, Kr and Xe from non-relativistic RPAE calculations are shown with dots. Similarly colored solid lines represent the HF scattering phase in the corresponding dominant photoionization channel. The dotted lines are used to visualize the asymptotics of the short range phase in the zero kinetic energy limit.

TABLE II: Quantum defect parameters from the discrete binding energy fit $E_{\underline{n}_i l_i n l} = -Z_{\text{eff}}^2 / (n - \mu)^2$ with $Z_{\text{eff}} = 1$ compared with the logarithmic phase interpolation to the 1 eV photoelectron kinetic energy for various Rydberg series. The hole state $n l$ is underlined in the table captions.

	Neon			Argon				Krypton					Xenon				
$\underline{n}_i l_i n l$	<u>1snp</u>	<u>2snp</u>	<u>2pnd</u>	<u>1snp</u>	<u>2snp</u>	<u>3snp</u>	<u>2pnd</u>	<u>2snp</u>	<u>3snp</u>	<u>2pnd</u>	<u>3pnd</u>	<u>3dnf</u>	<u>2snp</u>	<u>3snp</u>	<u>2pnd</u>	<u>3pnd</u>	<u>3dnf</u>
N_l	1	1	0	2	2	2	0	3	3	1	1	0	4	4	2	2	0
μ	1.07	0.85	0.011	1.97	1.86	1.67	0.53	2.84	2.76	1.58	1.51	0.004	3.77	3.72	2.90	2.90	0.006
a/π	0.99	0.88	0.11	2.13	2.22	2.23	0.78	3.45	3.37	1.91	2.18	0.48	4.53	4.50	3.19	3.32	1.04

Coulomb center and their interaction with the neighbouring subshells is generally relatively weak. In Ne, even the innermost 1s phase shows noticeable deviation of the RPAE and HF phases near threshold. This deviation is of the same size as in the valence 2s shell. In Ar, all the HF and RPAE phases are rather close except for the 3s shell which demonstrates a very strong deviation due to profound correlation with the outer 3p shell. This result is already acknowledged in our previous work [20]. In Kr, the inner 2s, 2p and 3s phases are well described by

the HF model while the intermediate 3p and 3d electrons show noticeable deviation of the HF and RPAE results. In Xe, all the phases shown are HF-like because we only studied the innermost shells.

Note that, in all cases shown, the phases exhibit a monotone increase from threshold at the lower energies, owing to the dominance of the Coulomb phase near threshold. At the higher energies, as mentioned above, the Coulomb phase rapidly approaches zero, so the behavior of the total phase is dominated by the phase gener-

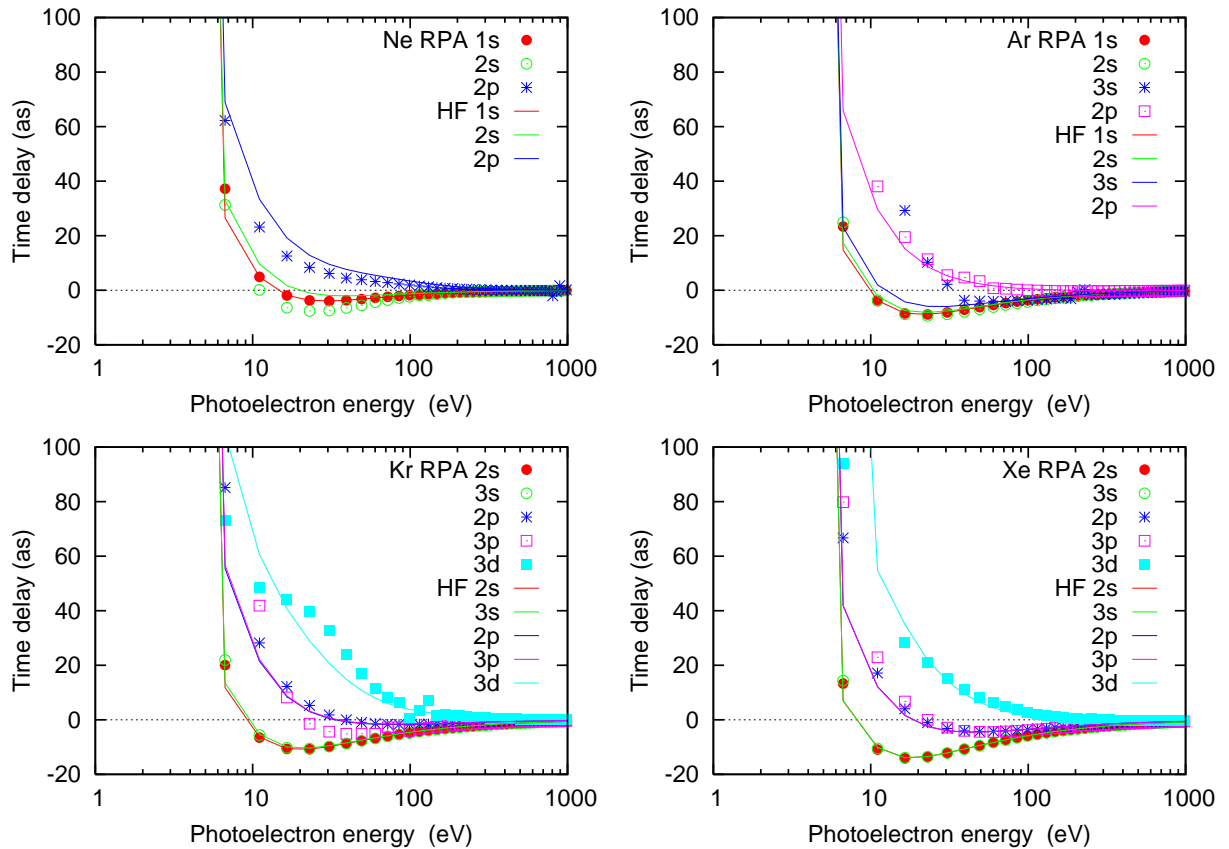


FIG. 4: (Color online) Photoelectron group delays (Wigner time delays) in various shells of Ne, Ar, Kr and Xe from non-relativistic RPAE calculations are shown with dots. Similarly colored solid lines represent the analogous HF results summed over all the photoionization channels.

ated by the short-range potential. For the $ns \rightarrow \epsilon p$ channels this phase in monotone decreasing, and this leads to the situation seen in Fig. 3 where the total phases in the $ns \rightarrow \epsilon p$ channels increase rapidly from threshold, reach a maximum, and then decrease monotonically towards zero, with increasing energy. The $np \rightarrow \epsilon d$ channels, on the other hand, do not all behave in the same manner. For Ne and Ar, the short range d -wave phase never

reaches an appreciable value, so the turnover of the total phase occurs at a rather large value of the energy, larger than is displayed in Fig. 3. For Kr and Xe, on the other hand, there are shape resonances in the $np \rightarrow \epsilon d$ channels [32, 33] so the short range phase do reach appreciable values; as a result, the behavior of the total phases are just like the $ns \rightarrow \epsilon p$ channels. And for the $3d \rightarrow \epsilon f$ channels, the turnovers again are well beyond the plotted values.

C. Time delay

Photoelectron group delays (Wigner time delays) in various shells of Ne and Ar (top) and Kr and Xe (bottom) are shown in Fig. 4. The typical behavior of the group delay can be understood from the phase analysis of the previous section. The Coulomb singularity, Eq. (6), drives the phase to large negative values as the photoelectron energy decreases near the threshold. Hence the Wigner time delay becomes very large and positive $\tau_W \propto 1/E^{3/2} \ln(1/E)$. We note that the same energy dependence is carried by the CLC corrections

$\tau_{CLC} \propto 1/E^{3/2} \ln(aE + b)$ [25, 34, 35] but these corrections are *negative*. This results in a large and negative net atomic time delay $\tau_a = \tau_W + \tau_{CLC}$ when the time delay measurement is taken very close to the threshold. However, the Wigner component τ_W cannot be entirely neglected when analyzing the near-threshold time delay measurement results as in [15].

At modest photoelectron energies, the phase bends over as it becomes influenced by the short-range HF component. Somewhere near this point, the time delay changes its sign and becomes negative. The exception is the np -shells in Ne and Ar and the nd -shells in Kr

and Xe where the photoelectrons in the dominant $l_i + 1$ photoionization channel do not have bound states with matching orbital character in the ionized core. At large photoelectron energies, the time delay gradually goes to zero because the long range Coulomb contribution to the phase becomes vanishingly small and the short range HF contribution approaches zero extremely slowly, so slowly that its derivative also becomes vanishingly small.

The deviation of the HF and RPAE phases is exemplified in the time delay plots. It is most clearly visible in the valence shells of Ne and Ar, along with the $3d$ sub-shell of Kr. In all cases, however, the HF and RPAE time delays are qualitatively similar. To summarize, the low (kinetic) energy time delay is dominated by the Coulomb phase. The high energy region seems to be dominated by the short range HF phase; correlation in the form of interchannel coupling become relatively unimportant at high energy (except possibly near inner-shell thresholds). Thus, correlation plays no role in the qualitative behavior of the time delay vs. energy, but it can affect the quantitative behavior.

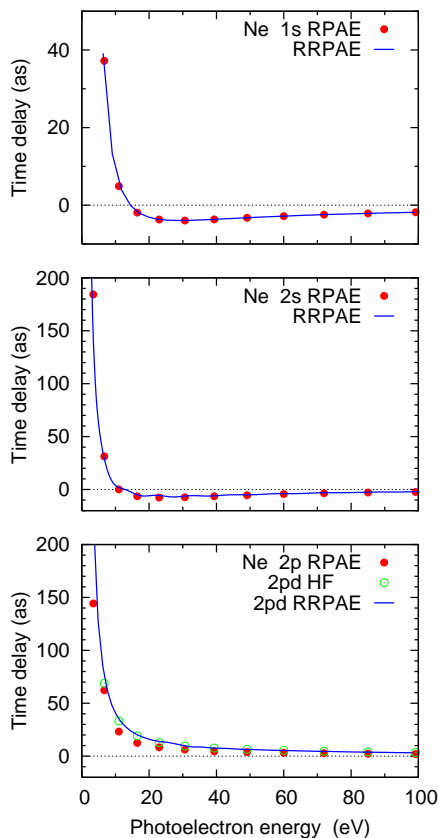


FIG. 5: (Color online) Time delay in photoionization of the $1s$, $2s$ and $2p$ shells of Ne. Non-relativistic RPAE results (red filled circles) are compared with RRPAAE results (blue solid lines) for $1s \rightarrow \epsilon p$, $2s \rightarrow \epsilon p$ and $2p \rightarrow \epsilon d$ ionization channels. The HF calculation for the $2p \rightarrow \epsilon d$ is shown by the (green) open circles.

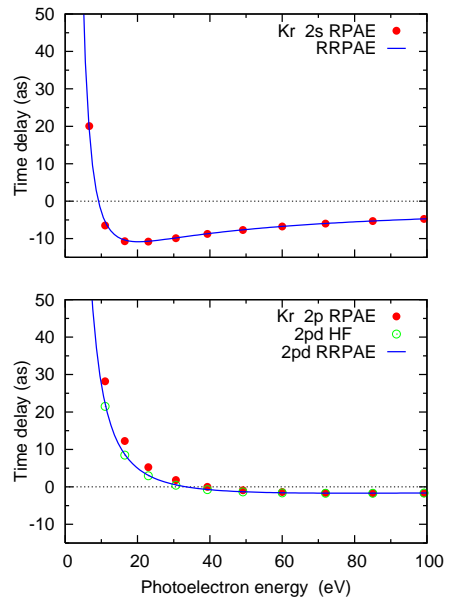


FIG. 6: (Color online) Time delay in photoionization of the $2s$ and $2p$ shells of Kr. Non-relativistic RPAE results (red filled circles) are compared with RRPAAE results (blue solid lines) for $2s \rightarrow \epsilon p$ and $2p \rightarrow \epsilon d$ ionization channels. The HF calculation for the $2p \rightarrow \epsilon d$ is shown by the (green) open circles.

D. Comparison of RPAE and RRPAAE calculations

To elucidate the role of relativistic effects in time delay calculations, we make a comparison of the RPAE and RRPAAE results. This comparison for Ne, Kr and Xe is shown in Fig. 5, Fig. 6 and Fig. 7, respectively.

Non surprisingly, for such a light atom as Ne, there is no visible deviation between the RPAE and RRPA results in the $1s$ and $2s$ ionization. This deviation can be detected in the $2p$ shell ionization. This is largely because the RPAE calculation includes the sum of the two photoionization channels $2p \rightarrow \epsilon d$ and $2p \rightarrow \epsilon s$ whereas the RRPA result includes only the stronger $2p \rightarrow \epsilon d$ channel. To match this calculation, we make a comparison with the analogous HF result and agreement is much improved.

A similar comparison for Kr and Xe is made in Fig. 6 and Fig. 7, respectively. Even though, these atoms are significantly heavier than Ne, relativistic effects do not show up in the time delay of the $2s$ shell and both the RPAE and RRPA results practically coincide. The difference between the two calculations for the $2p$ shell can again be attributed to the partial summation of the photoionization channels. When only one $2p \rightarrow \epsilon d$ channel is included into the HF calculation, it becomes very close to the analogous RRPA result.

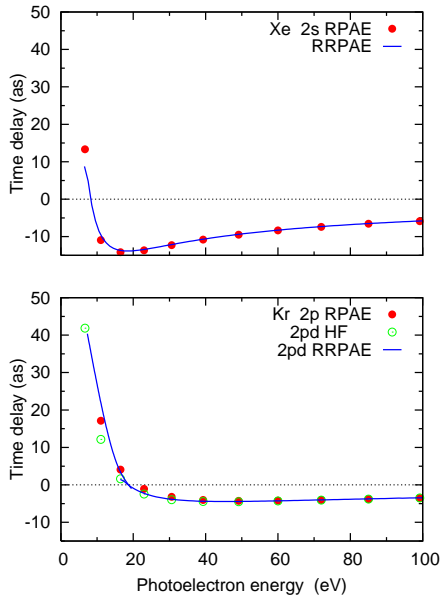


FIG. 7: (Color online) Time delay in photoionization of the $2s$ and $2p$ shells of Xe. Non-relativistic RPAE results (red filled circles) are compared with RRPAE results (blue solid lines) for $2s \rightarrow \epsilon p$ and $2p \rightarrow \epsilon d$ ionization channels. The HF calculation for the $2p \rightarrow \epsilon d$ is shown by the (green) open circles.

IV. CONCLUSION

We conduct a systematic study of the dipole phase and the photoelectron group delay (Wigner time delay) in inner shell photoionization of noble gas atoms from Ne to Xe. Our study encompasses the tender X-ray spectral range and extends to 1 keV photoelectron energy. We employ both the relativistic and non-relativistic versions of the random phase approximation with exchange. We identify the long range Coulomb and short range Hartree-Fock contributions to the dipole phase which governs the Wigner time delay variation from the threshold to the whole range of photoelectron energies. The inter-shell correlations (interchannel coupling) are found significant in all shells of Ne, the $3s$ subshell of Ar and $3d$ -subshell of Kr. Relativistic effects do not significantly change the time delay results.

We hope that our numerical results will serve as a useful benchmark in time resolved studies of atomic ionization. Because the correlations do not play a determinative role in the photoionization of inner atomic shells, relatively simple Hartree-Fock or Dirac-Fock calculations may be sufficient for time delay evaluation that can be performed for a wide range of atoms both with closed and open shells. Because the inner shells are not strongly influenced by the chemical environment, similar time delays will be observed in corresponding inner shells of molecules and solids. Thus, it is expected that the phenomenology found for the photoionization time delay and

the phase of the dipole amplitudes of noble gas atoms will be generally applicable to the qualitative behavior of inner shells of other atoms, both open- and closed-shell, molecules and solids as well.

Acknowledgments

A.K. acknowledges support by the Australian Research Council in the form of the Discovery grant DP120101805. V.K.D. acknowledges the support of NSF under grant No. PHY-1305085. S.T.M. acknowledges the support of

the Chemical Sciences, Geosciences and Biosciences Division, Office of Basic Energy Sciences, Office of Science, US Department of Energy under Grant No. DE-FG02-03ER15428. P.C.D. appreciates the support of the grant from the Department of Science and Technology, Government of India.

-
- [1] J. Itatani, F. Quéré, G. L. Yudin, M. Y. Ivanov, F. Krausz, and P. B. Corkum, *Attosecond streak camera*, Phys. Rev. Lett. **88**, 173903 (2002).
- [2] M. Schultze *et al.*, *Delay in Photoemission*, Science **328**(5986), 1658 (2010).
- [3] L. Eisenbud, *Formal properties of nuclear collisions*, Ph.D. thesis, Princeton University (1948).
- [4] E. P. Wigner, *Lower limit for the energy derivative of the scattering phase shift*, Phys. Rev. **98**(1), 145 (1955).
- [5] F. T. Smith, *Lifetime matrix in collision theory*, Phys. Rev. **118**, 349 (1960).
- [6] H. Muller, *Reconstruction of attosecond harmonic beating by interference of two-photon transitions*, Applied Physics B: Lasers and Optics **74**, s17 (2002), 10.1007/s00340-002-0894-8.
- [7] Klünder *et al.* K., *Probing single-photon ionization on the attosecond time scale*, Phys. Rev. Lett. **106**(14), 143002 (2011).
- [8] D. Guénot, K. Klünder, C. L. Arnold, D. Kroon, J. M. Dahlström, M. Miranda, T. Fordell, M. Gisselbrecht, P. Johnsson, J. Mauritsson, *et al.*, *Photoemission-time-delay measurements and calculations close to the 3s-ionization-cross-section minimum in Ar*, Phys. Rev. A **85**, 053424 (2012).
- [9] S. B. Schoun, R. Chirla, J. Wheeler, C. Roedig, P. Agostini, L. F. DiMauro, K. J. Schafer, and M. B. Gaarde, *Attosecond pulse shaping around a Cooper minimum*, Phys. Rev. Lett. **112**, 153001 (2014).
- [10] M. Negro, D. Faccialá, B. Bruner, M. Devetta, S. D. Silvestri, N. Dudovich, S. Pabst, R. Santra, H. Soifer, S. Stagira, *et al.*, *Probing Xenon Electronic Structure by Two-Color Driven High-Order Harmonic Generation*, *Ultrafast Phenomena XIX* (Springer, Okinawa, Japan, 2014), pp. 7–10, Proceedings in Physics.
- [11] T. Popmintchev, M.-C. Chen, P. Arpin, M. M. Murnane, and H. C. Kapteyn, *The attosecond nonlinear optics of bright coherent x-ray generation*, Nat Photon **4**, 822 (2010).
- [12] B. Wolter, M. G. Pullen, M. Baudisch, M. Sciafani, M. Hemmer, A. Senfleben, C. D. Schröter, J. Ullrich, R. Moshhammer, and J. Biegert, *Strong-field physics with mid-IR fields*, Phys. Rev. X **5**, 021034 (2015).
- [13] J. Biegert (2015), private communication.
- [14] G. Schmid, *XUV-pump THz-probe experiments on neon at the free-electron laser in Hamburg*, Master's thesis, Ruprecht-Karls-Universität, Heidelberg (2013), URL <http://hdl.handle.net/11858/00-001M-0000-0014-9DBB-7>.
- [15] G. Schmid *et al.*, *Terahertz field induced time shifts in atomic photoemission*, Phys. Rev. Lett. p. to be submitted (2015).
- [16] U. Fruhling, M. Wieland, M. Gensch, T. Gebert, B. Schutte, M. Krikunova, R. Kalms, F. Budzyn, O. Grimm, J. Rossbach, *et al.*, *Single-shot terahertz-field-driven x-ray streak camera*, Nat Photon **3**, 523 (2009), 10.1038/nphoton.2009.160.
- [17] I. Grguras, A. R. Maier, C. Behrens, T. Mazza, T. J. Kelly, P. Radcliffe, S. Dusterer, A. K. Kazansky, N. M. Kabachnik, T. Tschentscher, *et al.*, *Ultrafast x-ray pulse characterization at free-electron lasers*, Nat Photon **6**, 852 (2012).
- [18] P. N. Juranić, A. Stepanov, R. Ischebeck, V. Schlott, C. Pradervand, L. Patthey, M. Radović, I. Gorgisyan, L. Rivkin, C. P. Hauri, *et al.*, *High-precision x-ray FEL pulse arrival time measurements at SACLA by a THz streak camera with Xe clusters*, Opt. Express **22**(24), 30004 (2014).
- [19] I. Gorgisyan, R. Ischebeck, E. P. Costa, S. Reiche, L. Rivkin, and P. Juranic, *Simulation of fel pulse length calculation with THz streaking method*, J. Synchr. Rad. p. to be submitted (2015).
- [20] A. S. Kheifets, *Time delay in valence-shell photoionization of noble-gas atoms*, Phys. Rev. A **87**, 063404 (2013).
- [21] A. C. Thompson, D. T. Attwood, E. M. Gullikson, M. R. Howells, J. B. Kortright, A. L. Robinson, and J. H. Underwood, *X-ray data booklet* (Center for X-ray Optics and Advanced Light Source, Lawrence Berkeley National Laboratory, 2009).
- [22] S. Saha, A. Mandal, J. Jose, H. R. Varma, P. C. Deshmukh, A. S. Kheifets, V. K. Dolmatov, and S. T. Manson, *Relativistic effects in photoionization time delay near the Cooper minimum of noble-gas atoms*, Phys. Rev. A **90**, 053406 (2014).
- [23] J. Berkowitz, *Photoabsorption, Photoionization, and Photoelectron Spectroscopy* (Elsevier Science, 2012).
- [24] I. Band, Y. Kharitonov, and M. Trzhaskovskaya, *Photoionization cross sections and photoelectron angular distributions for x-ray line energies in the range 0.132-509 keV targets: $1 \leq Z \leq 100$* , Atomic Data and Nuclear Data Tables **23**(5), 443 (1979).
- [25] R. Pazourek, S. Nagele, and J. Burgdorfer, *Time-resolved photoemission on the attosecond scale: opportunities and challenges*, Faraday Discuss. **163**, 353 (2013).
- [26] J. Dahlström, D. Guénot, K. Klünder, M. Gisselbrecht, J. Mauritsson, A. L. Huillier, A. Maquet, and R. Taïeb, *Theory of attosecond delays in laser-assisted photoionization*, Chem. Phys. **414**, 53 (2012).
- [27] L. V. Chernysheva, N. A. Cherepkov, and V. Radojevic, *Self-consistent field Hartree-Fock program for atoms*, Comp. Phys. Comm. **11**, 57 (1976).
- [28] L. V. Chernysheva, N. A. Cherepkov, and V. Radojevic, *Frozen core hartree-fock programm for atomic discrete and continuous states*, Comp. Phys. Comm. **18**, 87 (1979).
- [29] U. Fano, *Propensity rules: An analytical approach*, Phys. Rev. A **32**, 617 (1985).

- [30] J. C. A. Barata, L. F. Canto, and M. S. Hussein, *New asymptotic formulae for the point Coulomb phase shift*, Brazilian J. Phys. **41**, 50 (2011).
- [31] L. Rosenberg, *Levinson-Seatton theorem for potentials with an attractive Coulomb tail*, Phys. Rev. A **52**(5), 3824 (1995).
- [32] D. J. Kennedy and S. T. Manson, *Photoionization of the noble gases: Cross sections and angular distributions*, Phys. Rev. A **5**, 227 (1972).
- [33] S. T. Manson, *Dependence of the phase shift on energy and atomic number for electron scattering by atomic fields*, Phys. Rev. **182**, 97 (1969).
- [34] V. V. Serov, V. L. Derbov, and T. A. Sergeeva, *Interpretation of time delay in the ionization of two-center systems*, Phys. Rev. A **87**, 063414 (2013).
- [35] M. Ivanov and O. Smirnova, *How accurate is the attosecond streak camera?*, Phys. Rev. Lett. **107**, 213605 (2011).